

1 ***Precision medicine for pandemics: stratification of COVID-19 molecular***
2 ***phenotypes defined by topological analysis of global blood gene expression.***

3
4 Rebekah Penrice-Randal ^{1,2}, Fabio Strazzeri ¹, Benoit Ernst ³, Brice Van Eeckhout ⁴,
5 Julien Guiot ³, Anna Julie Peired ⁵, Cosimo Nardi ⁵, Erika Parkinson ¹, Monique Henket
6 ³, Alicia Staderoli ³, Elora Guglielmi ³, Anne-Françoise Dive ³, Laurie Giltay ³, Sara
7 Tomassetti ⁶, Rebecca Baker ⁷, Kit Howard ⁷, Catherine Hartley ², Tessa Prince ²,
8 Thomas Kleyntssens ⁴, Ratko Djukanovic ^{8,9}, Tristan Clark ^{8,9}, Diana Baralle ^{9,10}, Scott
9 S Wagers ¹¹, Xiaodan Xing ¹², Yang Nan ¹², Shiyi Wang ¹², Simon Walsh ¹³, Guang
10 Yang ¹², Paul J Skipp ^{1,14}, Julian A Hiscox ^{2,15,16}, James P R Schofield ¹.

11
12
13 **Affiliations:**

14 ¹TopMD Precision Medicine Ltd, Southampton, United Kingdom

15 ²Institute of Infection, Veterinary and Ecological Sciences, University of Liverpool,
16 Liverpool, UK.

17 ³Department of Respiratory Medicine, University Hospital of Liège, Liège, Belgium.

18
19 ⁴Comunicare Solutions, Liège, Belgium.

20
21 ⁵Department of Experimental and Clinical Biomedical Sciences “Mario Serio”,
22 University of Florence, Viale Morgagni 50, 50134 Florence, Italy.

23
24 ⁶Department of Clinical and Experimental Medicine, Careggi University Hospital,
25 Largo Brambilla 3, 50134 Florence, IT

26
27 ⁷Clinical Data Interchange Standards Consortium (CDISC), Austin, TX, United States
28 of America

29
30 ⁸Clinical and Experimental Sciences, Faculty of Medicine, University of
31 Southampton, Southampton, United Kingdom

32
NOTE: This preprint reports new research that has not been certified by peer review and should not be used to guide clinical practice.

33 ⁹National Institute for Health Research Southampton Biomedical Research Centre,
34 Southampton, United Kingdom

35

36 ¹⁰School of Human Development and Health, Faculty of Medicine, University of
37 Southampton, Southampton, United Kingdom

38

39 ¹¹BioSci Consulting, Maasmechelen, Belgium

40

41 ¹²Department of Bioengineering and Imperial-X, Imperial College London

42

43 ¹³National Heart and Lung Institute, Imperial College London

44

45 ¹⁴School of Biological Sciences, University of Southampton, Southampton, UK

46

47 ¹⁵NIHR Health Protection Research Unit in Emerging and Zoonotic Infections,
48 Liverpool, UK.

49

50 ¹⁶A*STAR Infectious Diseases Laboratories (A*STAR ID Labs), Agency for Science,
51 Technology and Research (A*STAR), Singapore.

52

53 **Abstract:**

54 Precision medicine offers a promising avenue for better therapeutic responses to
55 pandemics such as COVID-19. This study leverages independent patient cohorts in
56 Florence and Liège gathered under the umbrella of the DRAGON consortium for the
57 stratification of molecular phenotypes associated with COVID-19 using topological
58 analysis of global blood gene expression. Whole blood from 173 patients was collected
59 and RNA was sequenced on the Novaseq platform. Molecular phenotypes were
60 defined through topological analysis of gene expression relative to the biological
61 network using the TopMD algorithm. The two cohorts from Florence and Liège allowed
62 for independent validation of the findings in this study. Clustering of the topological
63 maps of differential pathway activation revealed three distinct molecular phenotypes
64 of COVID-19 in the Florence patient cohort, which were also observed in the Liège
65 cohort.

66

67 Cluster 1 was characterised by high activation of pathways associated with ESC
68 pluripotency, NRF2, and TGF- β receptor signalling. Cluster 2 displayed high activation
69 of pathways including focal adhesion-PI3K-Akt-mTOR signalling and type I interferon
70 induction and signalling, while Cluster 3 exhibited low IRF7-related pathway activation.
71 TopMD was also used with the Drug-Gene Interaction Database (DGIdb), revealing
72 pharmaceutical interventions targeting mechanisms across multiple phenotypes and
73 individuals.

74

75 The data illustrates the utility of molecular phenotyping from topological analysis of
76 blood gene expression, and holds promise for informing personalised therapeutic
77 strategies not only for COVID-19 but also for Disease X. Its potential transferability
78 across multiple diseases highlights the value in pandemic response efforts, offering
79 insights before large-scale clinical studies are initiated.

80

81

82 **Introduction:**

83

84 The ongoing challenges of COVID-19, triggered by the emergence of SARS-CoV-2,
85 necessitate a detailed understanding of disease heterogeneity. Despite extensive
86 research characterising the host response to SARS-CoV-2 through pre-clinical (1, 2),
87 and clinical (3-6) functional genomic data, there have been limited approaches that
88 have used data from and encompassed the range of symptom severity, disease
89 heterogeneity and delivered personalised medicine.

90

91 Examination of gene expression patterns in blood has been used in previous studies
92 to identify molecular phenotypes associated with different disease profiles in several
93 emerging viral infections including Ebola virus (EBOV) (7) and SARS-CoV-2 (1, 2, 4,
94 5), as well as more endemic infections such as influenza virus (8). Medical
95 countermeasures focus on either reducing viral load through anti-virals. These target
96 viral biology or modulate the host response to infection to reduce sequelae such as
97 inflammation. For many viruses there is a clear correlation between viral load, disease
98 severity and outcome (survival/death). This is best typified by the Ebola virus where
99 low viral loads correlate with survival and high viral loads correlate with death (9). For
100 SARS-CoV-2 this correlation is less obvious. In animal models of disease, such as the
101 ferret, viral load was correlated with symptomology (10); in humans, there is less data
102 to support an association between viral load and disease. However, studies have
103 shown that severe COVID-19 is associated with dysregulated immune pathology in
104 organs such as the lungs and the respiratory tract (3, 11).

105

106 With any emerging viral pathogen, direct acting antivirals take time to develop and
107 trial. Identifying therapeutics that can modulate the host response to reduce
108 symptomology remain a priority. Being able to rapidly characterise aberrations in host
109 pathways that lead to disease and marrying this with therapeutics on the FDA
110 approved list will enhance pandemic preparedness and rapid response. Therefore, a
111 deeper understanding of the host response can be used to guide the selection of host
112 directed medication countermeasures.

113

114

115

116 The field of digital health and precision medicine is rapidly evolving, with emerging
117 technologies and initiatives aimed at integrating diverse datasets to inform clinical
118 decision-making. In this study we offer a novel way to analyse complex data collected
119 by the DRAGON international consortium which enables rapid identification of targets
120 for treatment by novel and/or re-purposed drugs. Within DRAGON, efforts have been
121 made to harmonise data in digital healthcare, proposing guidelines for the integration
122 of clinical data from various modalities. (12). Additionally, an online platform has been
123 developed to host validated COVID-19 predictive models, facilitating their utilisation
124 by clinicians in real-time decision-making (13). However, challenges persist, as
125 evidenced by the limited success of outcome prediction models for COVID-19 patients
126 based on demographic and comorbidity data, which highlights the need for more
127 sophisticated approaches (14).

128

129 While omics data has been instrumental in advancing our understanding of SARS-
130 CoV-2 and COVID-19, its integration into digital health platforms for clinical decision-
131 making remains limited (15-17). Traditional molecular phenotyping approaches often
132 provide only shallow insights. In previous work, using topological analysis, we
133 demonstrated how gene expression data derived from whole blood at the time of
134 admission could predict ICU admission (5). However, the current study analysed the
135 blood transcriptomes of patients with COVID-19 as part of the DRAGON-EU
136 consortium and used TopMD, an algorithm that considers all available data across a
137 landscape of pathways, to characterize molecular phenotypes of COVID-19 patients
138 admitted to hospital. Pathways were identified that correlated with clinical disease in
139 the patient cohort. TopMD mapped pathways onto a database containing information
140 on FDA approved drugs and their known gene and pathway interactions to generate
141 a list of potential therapeutics for modulating severe COVID-19. The ability to rapidly
142 identify and therapeutically modulate host pathways responsible for disease with pre-
143 existing medical countermeasures will be important in the emergence of novel
144 diseases and future pandemics.

145

146 This study describes an analysis of the blood transcriptomes of patients with COVID-
147 19 admitted to hospital in Liège and Florence between February and July 2021, as
148 part of the DRAGON-EU consortium. Alongside collecting blood samples,
149 demographic and clinical observations were recorded; additionally, CT scan data were

150 obtained for a subset of these patients. We applied an unsupervised approach, in
151 which we characterised the molecular phenotypes of patients within this cohort. We
152 have previously reported the development of a gene signature in patients with COVID-
153 19, predictive of admission to ICU (5). This predictive signature revealed the activation
154 of pathways regulating epidermal growth factor receptor (EGFR) signalling,
155 peroxisome proliferator-activated receptor alpha (PPAR- α) signalling and transforming
156 growth factor beta (TGF- β) signalling. The observed molecular phenotype aligns with
157 the mechanisms implicated in pulmonary fibrosis, which is also associated with
158 increased severity of disease (18-20).

159

160

161

162 **Methods:**

163

164 **Study population and sample collection and ethics**

165 Blood samples were obtained from 132 patients severe enough to require admission
166 because of COVID-19 at Careggi University Hospital, Florence, Italy, and 41 from a
167 pre-defined, separate patient cohort in Liège, between February and July 2021. All
168 patients tested positive nasopharyngeal swab PCR for SARS-CoV-2 infection. Blood
169 samples were collected on Day 0 of hospital admission. The protocol was approved
170 by the ethics committee of the University Hospital of Liège (reference number 2021/89)
171 and the ethics committee of the UNIFI (#18085/OSS). Informed consent was obtained
172 for every participant.

173

174 **Ethical Approval statement**

175 The work described has been carried out in accordance with The Code of Ethics of
176 the World Medical Association (Declaration of Helsinki) for experiments involving
177 humans. All procedures were performed in compliance with relevant laws and
178 institutional guidelines and have been approved by the appropriate institutional
179 committees. Informed consent was obtained for every participant.

180 Clinical data were collected from the patients' electronic medical records by the
181 investigators, and included age, sex, BMI, comorbid conditions etc. The data were
182 then assembled using the Study Data Tabulation Model (SDTM) data format
183 developed by the Clinical Data Interchange Standards Consortium (CDISC).

184 **Chest CT analysis**

185 Out of the 173 patients with RNA sequencing data, chest CT data was obtained from
186 109 patients using a 128-detector multislice Spiral Computed Tomography (MSCT)
187 (Somatom Definition AS, Siemens Healthcare, Erlangen, Germany) applying the
188 following parameters: current × exposure time 150 mAs, tube voltage 100 kV, rotation
189 time 0.3 s, pitch 1.2 mm, pixel size 0.465 mm, beam collimation 128 × 0.6 mm, both
190 slice thickness and reconstruction 1 mm, and reconstruction kernel Bf70 very sharp.
191 Axial images were carried out from lung apexes to bases with patient at full inspiration
192 and breath hold. Post-processing, 1-mm-thick sections were reconstructed on
193 coronal and sagittal planes oriented on the tracheal plane. Intravenous contrast

194 medium was not administered. Chest CT images were displayed on a 24-inch medical
195 monitor with a 3-megapixel Barco display (Barco, Kortrijk, Belgium) and 2048 x 1536
196 resolution. The software programs originally implemented to MSCT were used for
197 image assessment. Images of each patient were evaluated for scan quality
198 considering inspiratory level and motion artifacts. Data pulled out from CT
199 examinations included CO-RADS, chest CT score, dominant pattern, and
200 typical/atypical findings. Specifically:

201 **CO-RADS**

202 CO-RADS score based on COVID-19 lung involvement and variable from 1 to
203 5, with higher values reflecting a greater level of suspicion of COVID-19
204 infection with lung involvement. CO-RADS is a score used to diagnose COVID-
205 19 and does not inevitably reproduce the severity of lung alterations. Low
206 scores corresponded to CT examinations with alterations less likely related to
207 COVID-19 infection. The 5-score CO-RADS scale is as follows: 1: very low level
208 of suspicion; 2: low level of suspicion; 3: equivocal findings; 4: high level of
209 suspicion; 5: very high level of suspicion.

210 **Chest CT score for lobe involvement**

211 Ranging from 0 to 5, namely 0: 0%; 1: <5%; 2: 5-25%; 3: 26-50%; 4: 51-75%;
212 5: >75%.

213 **Dominant chest CT pattern**

214 Evaluated in relation to the prevalent alterations among ground-glass opacities,
215 consolidations, ground-glass opacities together with consolidations, crazy-
216 paving, and reverse halo, as defined by the Fleischner Society.

217 **Dominant chest CT distribution**

218 Lower lobes, upper lobes, peripheral, bronchocentric, dorsal, or diffuse.

219 **Additional COVID-19 related findings**

220 Represented by pleural thickening, vascular enlargement, subpleural sign, halo
221 sign air, bubble sign, perilobular pattern, and subpleural sparing.

222 **Additional findings not typical for COVID-19**

223 Represented by pleural effusion, pericardial effusion, lymphadenopathy,

224 cavitation, tree-in-bud, discrete small nodules, isolated lobar/segmental
225 consolidation, atelectasis, and smooth interlobular septal thickening.

226 **RNA extraction**

227 Total RNA was extracted from PAXgene BRT using the PAXgene Blood RNA Kit
228 (PreAnalytix), according to the manufacturer's protocol. Extracted RNA was stored at
229 -80°C until further use. Following the manufacturer's protocols, total RNA was used
230 as input material into the QIAseq FastSelect-rRNA/Globin Kit (Qiagen) protocol to
231 remove cytoplasmic and mitochondrial rRNA and globin mRNA with a fragmentation
232 time of 7 or 15 minutes. Subsequently the NEBNext® Ultra™ II Directional RNA Library
233 Prep Kit for Illumina® (New England Biolabs) was used to generate the RNA libraries,
234 followed by 11 or 13 cycles of amplification and purification using AMPure XP beads.
235 Each library was quantified using Qubit and the size distribution assessed using the
236 Agilent 2100 Bioanalyser and the final libraries were pooled in equimolar ratios.
237 Libraries were sequenced using 150 bp paired-end reads on an Illumina® NovaSeq
238 6000 (Illumina®, San Diego, USA).

239

240 **Bioinformatics**

241 Raw fastq files were trimmed using fastp (21). Trimmed paired end sequencing reads
242 were inputted into salmon (v1.5.2) using the -l A -validateMappings -SeqBias -gcBias
243 parameters (22). Quant files generated with salmon were imported into RStudio (4.1.1)
244 using tximport to infer gene expression (23). The edgeR package (3.34.1) was used
245 to normalise and scale sequencing libraries (24). Sequencing reads are available
246 under BioProject ID: PRJNA1085259 on Short Read Archive (SRA).

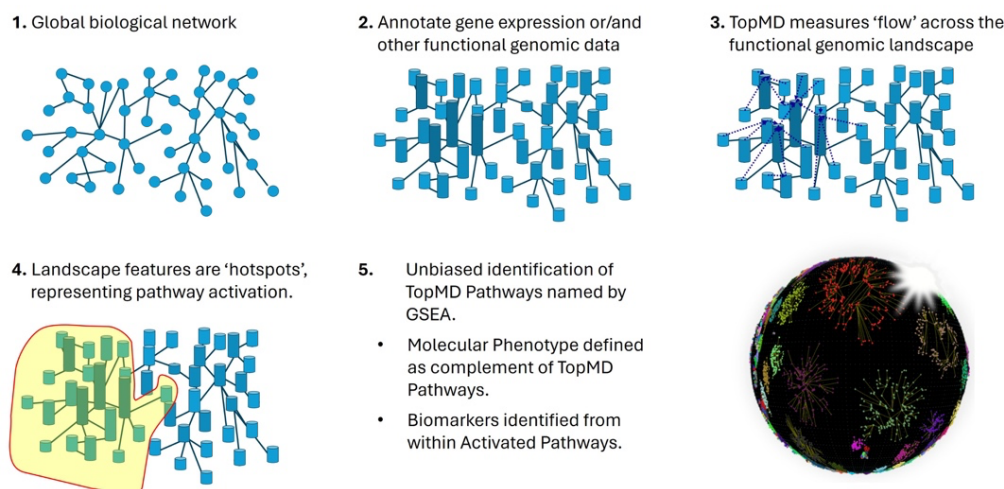
247

248 **Molecular phenotypes mapped by topological analysis**

249 Molecular phenotypes were mapped by topological analysis, using TopMD to measure
250 the shape of global gene expression relative to the biological network (TopMD Patent
251 number GB202306368D0). TopMD works in the following way: The biological network
252 used was an interaction network retrieved from the STRING database (25). The gene
253 nodes of the biological network were assigned vertices according to the measured
254 gene expression. The topological shape, or landscape, of this network is then
255 measured by TopMD's algorithm, clustering differential gene expression hotspots,
256 corresponding to modulated gene pathways. These pathways have 'volume'

257 comprising the sum of squared differential gene expression of clustered genes, where
258 the most differentially activated pathways have the highest pathway topological
259 volumes. The molecular phenotype is defined as the global profile of volumes of
260 differential pathway activation.

261



262

263

264 Drug interactions mapped by topological analysis

265

266 Due to the power of TopMD analysis we can group genes depending on their
267 expression values, this means that for each average expression of any cluster of
268 samples, and even on individual samples, we can extrapolate a tailored gene set of
269 activated gene-groups for such expression. These gene-groups can be then compared
270 to other gene sets, as in GSEA, as well against genes activated by specific drugs. To
271 do so, we utilised the Drug-Gene Interaction Database (26) obtained using genes or
272 gene products that are known or predicted to interact with drugs, and compared via a
273 binomial distribution test, the probability that an overlap between such genes and a
274 TopMD gene-group was random. This was measured using a p-value associated with
275 binomial statistic, together with other measures, such as the (Bonferroni) adjusted p-
276 value, a TopMD volume (combining volume of the shape with the statistical
277 significance of the drug-group combination) as well as an activation value, sum of the
278 Log2 fold-change of those genes belonging to both the drug associated gene set and
279 the TopMD group.

280

281 Regression

282 Regression analysis was carried out using a Logistic regression model with the
283 following optimisation problem:

284

$$\min_w C \sum_{i=1}^n s_i (-y_i \log(\hat{p}(X_i)) - (1 - y_i) \log(1 - \hat{p}(X_i))) + r(w)$$

285

286 Where X is the **pathway matrix** and y is the vector of the classification, 0 when the i-
287 th sample is in the class considered and 1 otherwise. We considered a regularisation
288 parameter C value of 1. For the penalisation term $r(w)$ for the regression weights w,
289 we considered an ElasticNet penalisation with the **l1 ratio** parameter value of 0.5

290

$$\frac{1-\rho}{2} w^T w + \rho \|w\|_1$$

291

292 The probability the i-th sample with **pathways values** equal to X_i is then:

$$\hat{p}(X_i) = \text{expit}(X_i w + w_0) = \frac{1}{1 + \exp(-X_i w - w_0)}$$

293

294 With w_0 the intercept. The python module used was **scikit-learn (version 1.4.1)** and
295 the algorithm used LogisticRegression function in the linear_model submodule.

296

297 We performed a 70/30 balanced split in the data [from both cohorts separately \(?\)](#), with
298 10 different splits. For each class we performed the regression based on a different
299 number of pathways, from 1 to 20, ranked in each split separately by their pathway
300 volume. For each regression model so obtained an average score of both training and
301 test splits was carried and the best model was selected using a max-min approach,
302 that is the best model was the one with highest value $\min(\text{AUC on Train}, \text{AUC on Test})$,
303 to avoid selecting models which were ill-performing on train splits, but instead for
304 random effects very well on test splits.

305

306

307 **Patient Clustering**

308 Pathway volumes were plotted on a PCA using PCAtools (v2.14.0), revealing 3 distinct
309 clusters, confirmed by K-means clustering, based on pathway activation against
310 healthy controls. The top ten (10%) of the PCA loadings were then extracted to identify

311 which pathways were driving cluster separation. To analyse differentially activated
312 pathways between patient clusters, we calculated the average volume, across each
313 cluster, of each pathway relative to the average of all the COVID-19 patients.

314

315 **Logistic Regression Receiver Operating Characteristic (LRROC) analysis using**
316 **patient clusters derived from the patient pathway volume matrix.**

317

318 The area under the ROC curve (AUC) is a measure of the model's ability to distinguish
319 between classes. A higher AUC indicates better discrimination and, consequently,
320 stronger patient clusters. LRROC for Florence Patients: LRROC analysis was
321 performed exclusively for Florence patients. The patient pathway volume matrix for
322 Florence patients was utilized to train the LRROC model. The output consisted of a
323 Receiver Operating Characteristic (ROC) curve, which depicted the classification
324 performance of patient clusters based on pathway volume. To evaluate the model's
325 generalization capability, the dataset was split into training and testing sets, and
326 separate ROC curves were generated for each.

327

328 Validation of clusters for Liège Patients: The LRROC model trained on Florence
329 patients was validated on Liège patients' data. Using the trained model, an additional
330 ROC curve was generated solely for Liège patients to assess the model's performance
331 in classifying Liège patient clusters based on pathway volume.

332

333

334 **Integration into digital health platform**

335 As a proof of concept, transcriptomics data and TopMD analysis were integrated with
336 a healthcare platform ran by Comunicare (27). This was to highlight the possibilities of
337 integrating omics data into healthcare and digital health platforms. Similar regression
338 analysis of COVID-19 blood transcriptomes, predicting ICU admission, performed
339 within the DRAGON scope (5) generated a linear model which is currently used to
340 generate prediction scores between 0 and 1, using TopMD analysis of each sample
341 submitted. In this way we can present TopMD analysis of individual samples compared
342 to a healthy baseline, which includes pathway activation information, together with a
343 similarity score to the ICU admitted average patient we extracted from previous data.

344 **Results:**

345

346 To investigate whether blood transcriptomic analysis coupled with a machine learning
347 approach underpinned by TopMD could be integrated with clinical data, RNA
348 sequencing was performed on peripheral blood obtained from 173 patients from Liège
349 (n=41) and Florence (n=132) gathered under the auspices of the DRAGON
350 consortium. A summary of the patient characteristics is described in Supplementary
351 Table 1. Within this cohort ten patients had fatal disease. As no outcome variables
352 within this cohort had power, an unsupervised approach was undertaken. Out of the
353 173 patients, 109 patients had matched CT data scored by clinicians. The data is
354 summarised in Supplementary Table 2. The majority of patients had a CORADS score
355 of high and very high, where 26% was equivocal, 4.6% low and 2.8% very low. The
356 CORADS score stands for "COVID-19 Reporting and Data System," which is a
357 classification system used in radiology to assess the likelihood of COVID-19 infection
358 based on chest imaging findings, typically on computed tomography (CT) scans. The
359 score categorizes imaging findings into different levels of suspicion for COVID-19,
360 ranging from very low to very high.

361

362 *Table 1: Characteristics of 132 patients from Florence included in the study,*
363 *including lab results at admission.*

Characteristic	N	N = 132 [†]
Died	132	
N		127 (96%)
Y		5 (3.8%)
Age	132	60 (50, 68)
Sex	132	
F		40 (30%)
M		92 (70%)
Non-invasive ventilation	132	

N	123 (93%)
Y	9 (6.8%)
Continuous positive airway pressure	132
N	129 (98%)
Y	3 (2.3%)
Tracheostomy	132
N	131 (99%)
Y	1 (0.8%)
High flow nasal cannula oxygen therapy	132
N	105 (80%)
Y	27 (20%)
Hypertension	132
N	77 (58%)
Y	55 (42%)
Malnutrition	132
N	131 (99%)
Y	1 (0.8%)
Cardiovascular disease	132
N	119 (90%)
Y	13 (9.8%)
Respiratory disease	132
N	118 (89%)
Y	14 (11%)

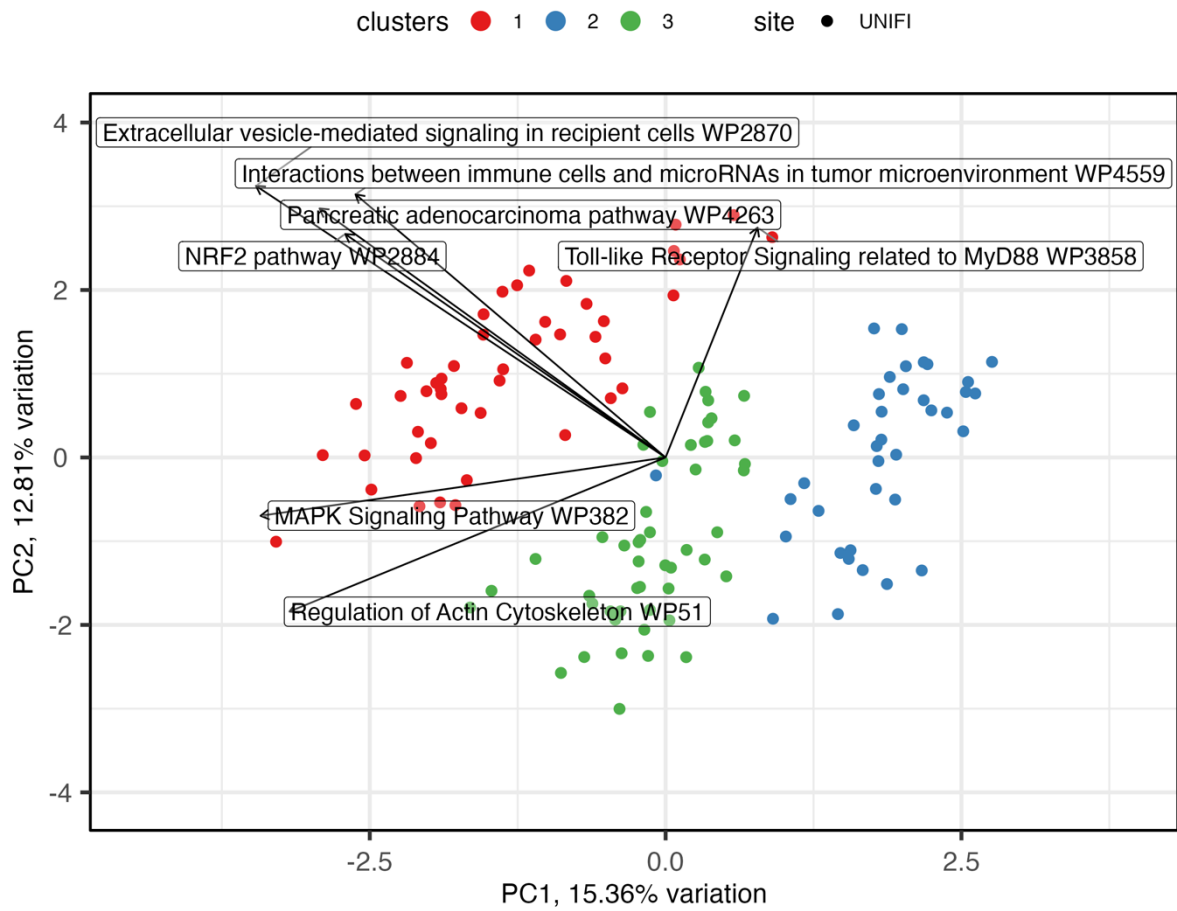
Cancer	132	
N		118 (89%)
Y		14 (11%)
Chronic kidney disease	132	
N		130 (98%)
Y		2 (1.5%)
Chronic hepatitis	132	
N		130 (98%)
Y		2 (1.5%)
Cerebrovascular disease	132	
N		125 (95%)
Y		7 (5.3%)
Chronic hematologic disease	132	
N		129 (98%)
Y		3 (2.3%)
Diastolic blood pressure (mmHg)	132	79 (70, 85)
Heart rate (BPM)	130	80 (75, 89)
Systolic blood pressure (mmHg)	132	125 (115, 140)
Temperature (°C)	131	36.50 (36.00, 37.20)
Weight (kg)	128	78 (70, 89)
Height (cm)	126	170 (165, 175)
Alanine aminotransferase (U/L)	128	27 (17, 39)
Aspartate aminotransferase (U/L)	64	31 (24, 46)

Bilirubin (mg/dL)	128	0.50 (0.30, 0.60)
Calcium (mg/dL)	96	4.50 (4.34, 4.63)
Creatinine (mg/dL)	130	0.83 (0.73, 0.95)
D-dimer (ng/mL)	91	728 (429, 1,091)
Direct bilirubin (mg/dL)	44	0.25 (0.17, 0.29)
Fibrinogen (mg/dL)	117	572 (446, 654)
Fraction of inspired oxygen (%)	127	28 (21, 36)
Hematocrit (%)	132	42.7 (39.7, 45.8)
Lactate dehydrogenase (U/L)	118	297 (247, 359)
Lactic acid (mg/dL)	102	9.0 (7.0, 11.9)
Leukocytes (10⁹/L)	132	6.2 (4.6, 7.7)
Lymphocytes (10⁹/L)	129	0.90 (0.68, 1.25)
Neutrophils (10⁹/L)	129	4.67 (3.08, 6.16)
Oxygen saturation (%)	109	96.10 (94.20, 97.70)
Partial pressure oxygen (mmHg)	131	74 (65, 87)
Partial pressure carbon dioxide (mmHg)	127	36.2 (34.0, 39.0)
Platelets (10⁹/L)	132	196 (156, 255)
Potassium (mmol/L)	128	3.85 (3.50, 4.10)
Procalcitonin (ug/L)	126	0.09 (0.06, 0.15)
Prothrombin time (seconds)	127	13.00 (12.30, 13.70)
Sodium (mmol/L)	129	137 (135, 140)
Urea nitrogen (g/L)	64	30 (30, 50)
[†] n (%); Median (IQR)		

365 **Patients form 3 clusters based on their pathway activation**

366

367 The RNA sequencing data was used to derive gene expression data (mRNA
368 identification and abundance) which was calculated using Salmon inferred with
369 Tximport in R, where values were converted into log2 counts per million (cpm). TopMD
370 was then employed to calculate the activation of pathways. To identify differences in
371 pathway activation across the cohort, activation data was plotted on a PCA which
372 revealed three distinct clusters of patients (Figure 1). The relationship between clinical
373 observations, demographics and CT scan data in each cluster was explored, and the
374 significant differences are reported in Table 3. Lactic acid was slightly higher in cluster
375 1 and 2 and lower in cluster 3. A higher proportion of respiratory disease was observed
376 in cluster 2 and the fraction of inspired oxygen was also higher in this cluster. Direct
377 bilirubin was also higher in cluster 2. The majority of those that died from COVID-19
378 were in cluster 2. CORADS scoring was unable to distinguish between the clusters at
379 a molecular level.



380

381 *Figure 1: TopMD pathway volumes of each patient in the Florence cohort, calculated*
382 *from a healthy plotted as a PCA plot. The data reveals three distinct clusters based on*
383 *pathway activation determined by kmeans.*

384 *Table 2: Patient characteristics that differ between the three clusters in the Florence*
 385 *cohort (p = <0.05).*

Characteristic	N	1, N = 46¹	2, N = 37¹	3, N = 49¹	p-value²
Lactic acid (mg/dL)	102	10.0 (7.7, 13.0)	10.0 (7.2, 12.0)	8.0 (5.3, 9.7)	0.008
Fraction of inspired oxygen (%)	127	28 (21, 36)	32 (27, 40)	28 (21, 29)	0.019
Died	132				0.032
N		46 (100%)	33 (89%)	48 (98%)	
Y		0 (0%)	4 (11%)	1 (2.0%)	
Respiratory disease	132				0.042
N		44 (96%)	29 (78%)	45 (92%)	
Y		2 (4.3%)	8 (22%)	4 (8.2%)	
Direct bilirubin (mg/dL)	44	0.20 (0.17, 0.27)	0.28 (0.24, 0.32)	0.20 (0.17, 0.28)	0.047

¹ n (%); Median (IQR)

² Fisher's exact test; Kruskal-Wallis rank sum test; Pearson's Chi-squared test

386

387 Molecular phenotype, Cluster 1, was characterised by high activation of pathways
 388 associated with ESC pluripotency, NRF2, and TGF-β receptor signalling (Figure 2).

389 Molecular phenotype, Cluster 2 displayed high activation of pathways including focal
 390 adhesion-PI3K-Akt-mTOR signalling and type I interferon induction and signalling,
 391 while Cluster 3 exhibited low IRF7-related pathway activation.

392

393 LRROC analysis was conducted on models trained using 70% of patients from the
394 Florence cohort, with test results evaluated on the remaining 30% of the Florence
395 cohort. The area under the ROC curve (AUCROC) values were found to be 0.84, 0.85,
396 and 0.72 for clusters Cluster 1, Cluster 2, and Cluster 3, respectively. Subsequently,
397 these clusters were validated in the Liège cohort (Supplementary Figure 1), yielding
398 AUCROC values of 0.76, 0.93, and 0.69 for Cluster 1, Cluster 2, and Cluster 3,
399 respectively (Supplementary Figure 2).

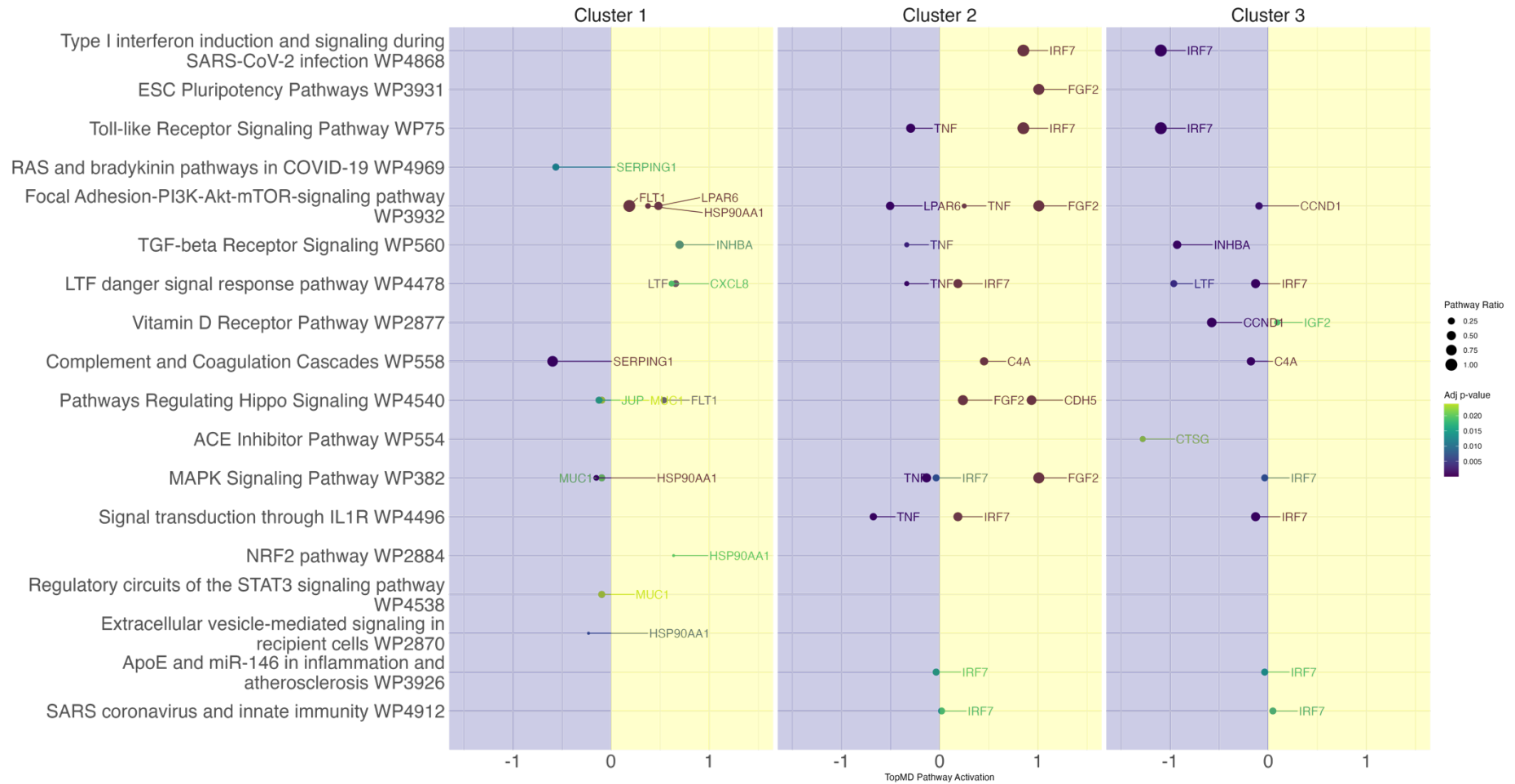
400

401

402 **Potential drug candidates are identified for each cluster**

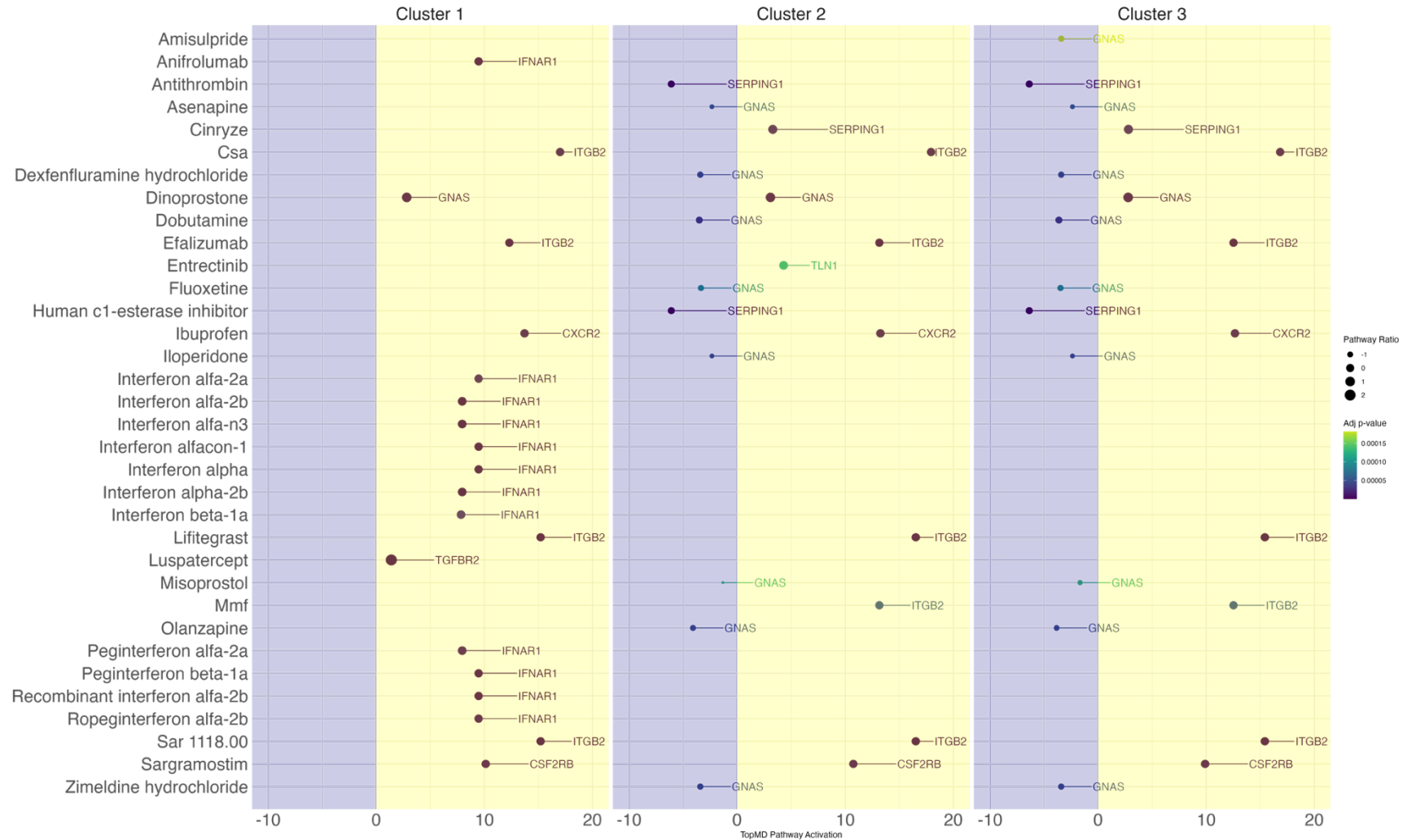
403 To identify potential drug candidates that modulate pathways identified in these
404 patient clusters, TopMD pathway activation was mapped onto the Drug-Gene
405 Interaction Database (Figure 3). This mapping revealed distinct drug targets for each
406 cluster, detailed in the supplementary table 4. This approach has a two-fold benefit:
407 informing potential clinical trials and informing underlying biological mechanisms
408 specific to each cluster. Interestingly, the pattern of pathway activation might also
409 provide insight into the potential benefits or drawbacks of specific therapies,
410 considering a drug's mechanism of action.

411 While all clusters shared targetable pathways led by genes such as ITGB2, GNAS,
412 and CXCR2, unique targets also emerged. Cluster 1 specifically identified IFNAR1,
413 TGFBR2, and CSF2RB, while cluster 2 added SERPING1 and TLN1. Notably, cluster
414 3 shared SERPING1 with cluster 2. These findings highlight both commonalities and
415 variations in potential therapeutic targets across the identified patient clusters.



416

417 *Figure 2: The average pathway volume for each cluster was considered in a TopMD enrichment analysis against the average pathway*
 418 *activation for the whole cohort to identify differentially activated pathways. The enrichment analysis was filtered by adjusted P value,*
 419 *then the top pathways were plotted. The pathways are annotated with the gene that leads the identified pathway. The dots are*
 420 *coloured by adjusted p-value and the size represents the proportion of genes identified within that pathway from TopMD analysis.*



421
 422 *Figure 3: TopMD enrichment analysis was mapped against the Drug-Gene Interaction Database, using a healthy baseline, revealing*
 423 *approved drugs that are known to target genes and their corresponding pathways. The top drug candidates are plotted based on*
 424 *adjusted p-value and pathway volume.*

425 Identification of pathways in fatal cases where intervention might 426 promote survival

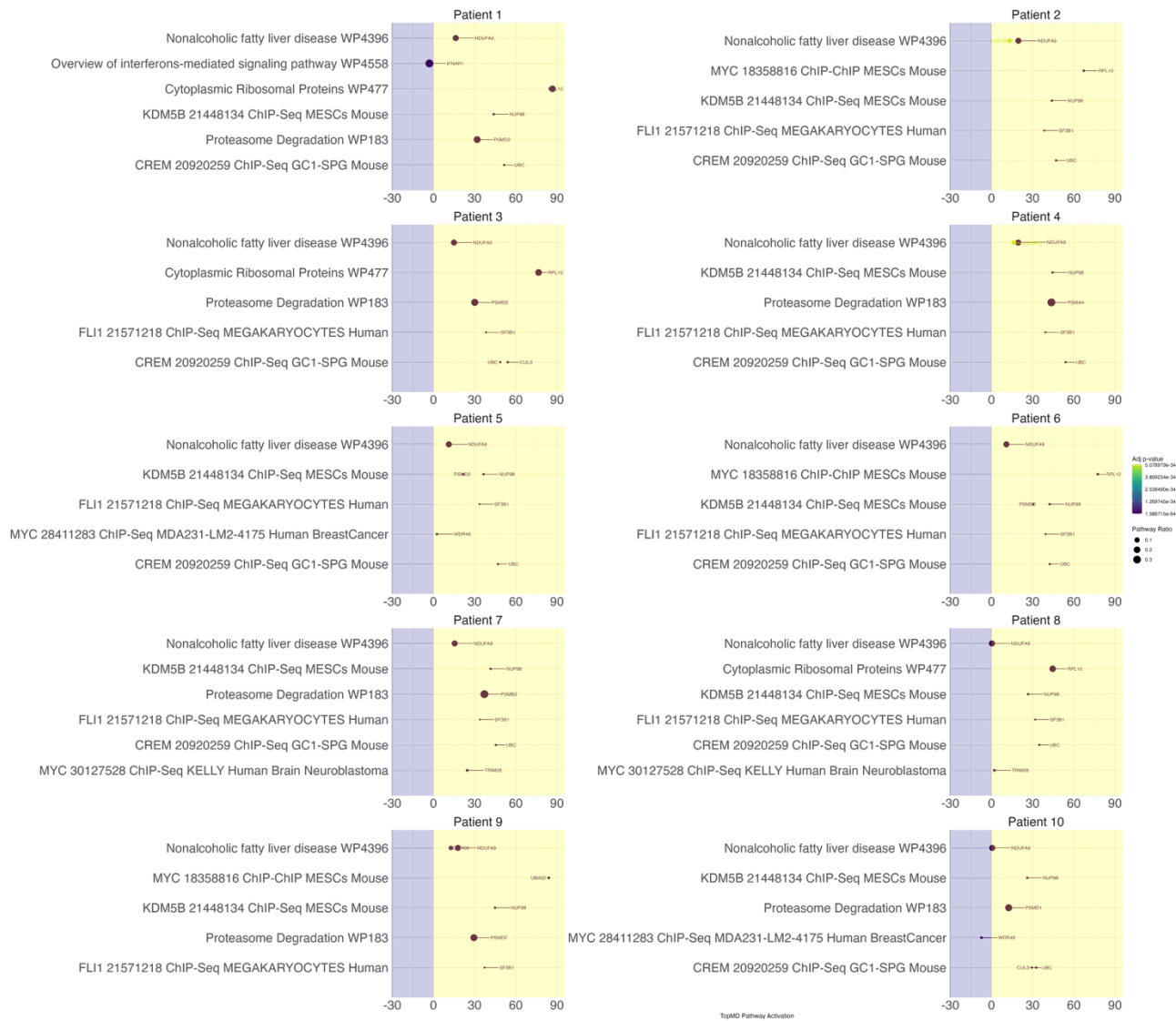
427 Due to limited sample size, we focused on the unsupervised analysis; however, to
428 show utility of investigating pathway activity in individuals, pathway analysis in the 10
429 deceased patients from the Florence and Liège cohort were observed. Unsurprisingly,
430 these patients exhibited advanced age and high comorbidity rates (cardiovascular:
431 70%, respiratory: 50%, malnutrition: 40%, hypertension: 90%, cerebrovascular: 30%,
432 chronic hepatitis: 40%). Interestingly, all 10 patients displayed a strong signal for
433 "nonalcoholic fatty liver disease" driven by the NDUFA9 and UQCRC2 genes (Figure
434 4).

435 Despite this shared pathway, individual analysis revealed heterogeneity among
436 deceased patients, highlighting the complex interplay between COVID-19,
437 comorbidities, and individual demographics on pathway activation.

438 Enrichment analysis identified potential therapeutic targets based on individual
439 pathway activation. All patients displayed potential targets including CXCR2 (Figure
440 5). Additionally, specific druggable pathways were identified for some patients,
441 including GNAS (multiple patients), ITGB2 (patients 2 & 6), CSF2RB (multiple
442 patients), SERPING1 (5 patients), PIK3CD (patient 5), TGFBR2 (patient 9), and
443 CUL4B (patient 10).

444

445



446

447

448 *Figure 4: The top 6 pathways enriched in fatal cases within the Florence and Liège*

449 *cohort using a healthy baseline.*

450

451

452

453

454

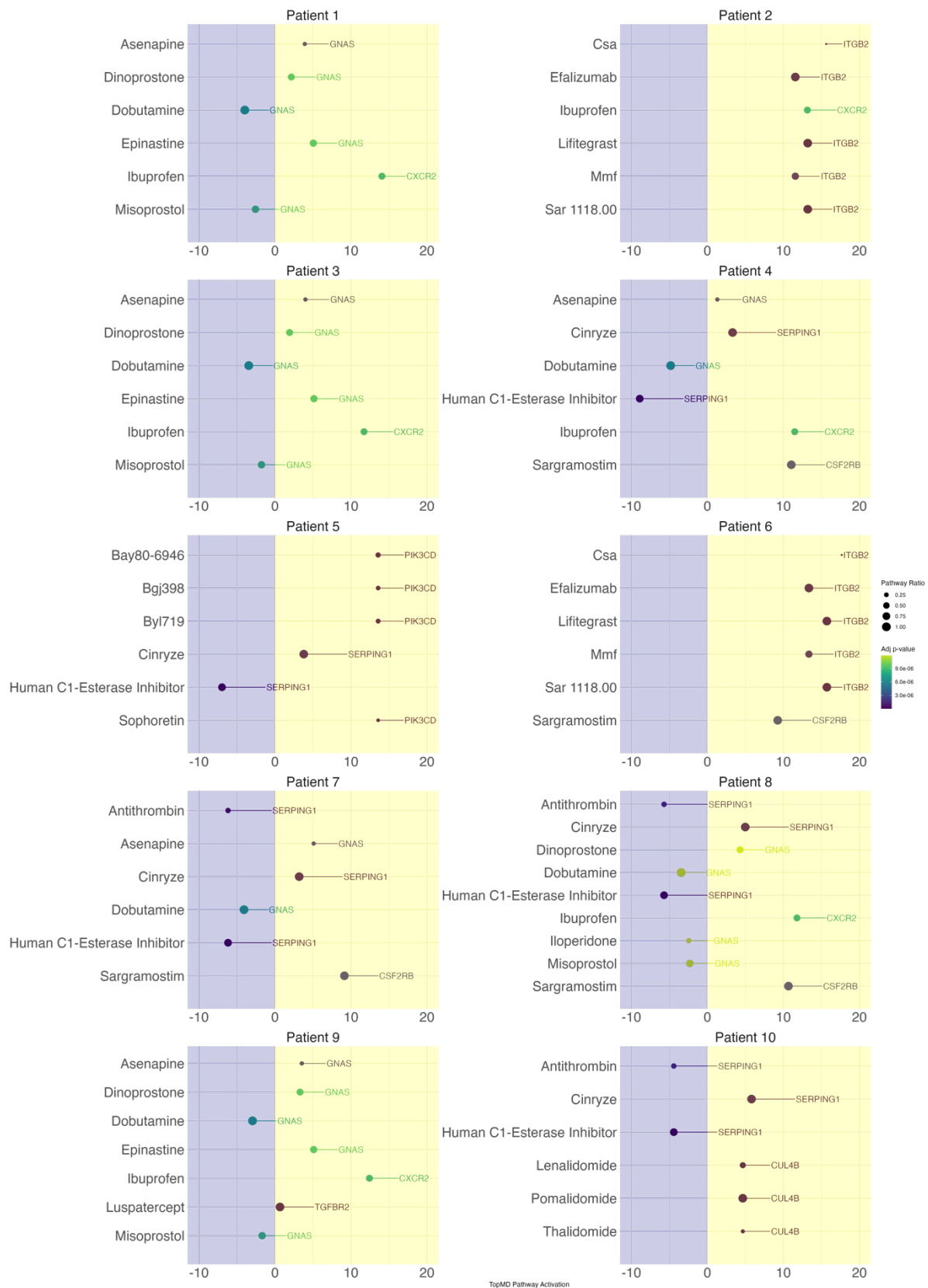
455

456

457

458

459



460

461 *Figure 5: The top significant drug candidates and peak genes that could potentially*
 462 *modulate the phenotype of the 10 fatal cases patients in the Florence and Liège*
 463 *cohort.*

464

465

466 **Discussion:**

467 Traditionally, molecular phenotyping requires data reduction and feature selection,
468 removing biological and technical ‘noise’, prior to pathway enrichment analysis, but
469 this leads to results which do not accurately represent the molecular phenotypes.
470 Topological analysis of global gene expression finds value in the low abundance
471 transcripts usually discarded as noise, as they represent the ‘foothills’ of largely
472 activated pathways in a comprehensive molecular landscape. By understanding the
473 molecular phenotype, it is possible to achieve more successful selection of
474 therapeutics, as medicines work at the molecular level as opposed to a clinical level
475 (28).

476
477 To redefine predictive models for patient outcomes and health trajectories, there is a
478 growing recognition of the importance of integrating complex datasets. This ranges
479 from biomarkers, clinical parameters to CT scans. For instance, a fully automated AI
480 framework was developed to extract features from chest CT scans for diagnosing
481 COVID-19. The model achieved 85.18% accuracy, enabling rapid and accurate
482 differentiation of COVID-19 from routine clinical conditions, facilitating timely
483 interventions and isolation procedures (29). Similarly, an AI-based analysis named
484 CACOVID-CT was implemented to automatically assess disease severity on chest CT
485 scans. Retrospective analysis of 476 patients revealed that quantitative
486 measurements, such as the percentage of affected lung area (% AA) and CT severity
487 score (CT-SS), correlated strongly with hospital length of stay, ICU admission,
488 mechanical ventilation, and in-hospital mortality. This tool proved effective in
489 identifying patients at higher risk of severe outcomes, facilitating patient management
490 and relieving the workload of radiologists (30).

491
492 Our study identified three distinct molecular phenotypes of COVID-19 molecular
493 through topological analysis of global blood gene expression. LRROC analysis
494 demonstrated strong discriminative power of the defined patient clusters tested in the
495 Florence and validated in the Liège cohort. This revealed insights into underlying
496 disease mechanisms, potentially guiding personalised therapeutic approaches.

497
498 The analysis using the TopMD algorithm assigned patients to three clusters. Some of
499 the clinical observations aligned with the defined clusters, including lactic acid

500 elevation in cluster 1 and 2 compared to cluster 3. Elevated lactic acid is known to be
501 associated with disease severity and mortality (31). Similarly, cluster 2 showed a
502 higher proportion of respiratory disease and required a higher fraction of inspired
503 oxygen. Additionally, this cluster exhibited elevated direct bilirubin, another potential
504 indicator of disease severity (32). Notably, the majority of those that died from COVID-
505 19 were in cluster 2 (n=4), although the overall number of fatalities in this cohort was
506 small (n=5).

507

508 Interestingly, the CORADS scoring system used for chest X-ray/CT severity
509 assessment, couldn't differentiate between the molecular clusters. This suggests
510 different molecular mechanisms might underlie similar clinical presentations, which
511 cannot be identified by CT scan. However, utilising higher resolution CT scan data,
512 such as continuous scoring systems offered by tools like Thirona, might provide more
513 granular insights compared to the categorical data used in this study (30).

514

515 Molecular differences were examined between each cluster by considering statistically
516 significant GSEA pathways with highest TopMD pathway volumes (Fig. 2). Cluster 1
517 displayed a reduction in pathways related to the renin-angiotensin system (RAS) and
518 bradykinin, implicated in COVID-19 pathogenesis (33). Additionally, an increase in
519 focal adhesion pathways, possibly indicating cellular changes related to tissue repair
520 and remodelling. Activation of the complement cascade, led by SERPING1, indicates
521 involvement in the immune response to the virus. Furthermore, an increase in the
522 TGF- β pathway, which regulates inflammation and tissue repair was also identified.
523 Additionally, a high activation of pathways associated with ESC pluripotency, NRF2,
524 and TGF- β receptor signalling. The ESC pluripotency pathway is implicated in tissue
525 repair and regeneration, suggesting a potential compensatory response to tissue
526 damage caused by the virus. NRF2 pathway activation may indicate an antioxidant
527 response to counteract oxidative stress induced by viral infection (34). TGF- β receptor
528 signalling, known for its role in regulating inflammation and fibrosis, may contribute to
529 tissue remodelling and fibrosis observed in severe COVID-19 cases (35). Also, cluster
530 1 exhibits low activation of pathways related to extracellular vesicle-mediated
531 signalling and complement and coagulation cascades. The decrease in extracellular
532 vesicle-mediated signalling may reflect impaired intercellular communication, while the

533 low activation of complement and coagulation cascades suggests a possible
534 dysregulated immune response and coagulopathy (36).

535

536 In cluster 2, high activation of pathways such as focal adhesion-PI3K-Akt-mTOR
537 signalling and type I interferon induction and signalling was observed, and has been
538 proposed as a potential therapeutic target in SARS-CoV-2 (37, 38) and MERS-CoV
539 (39). Focal adhesion pathway activation may indicate cellular responses to tissue
540 injury or viral invasion, while type I interferon induction and signalling reflect a strong
541 antiviral immune response (40). In contrast, cluster 3 shows opposite activity in IRF7-
542 related pathways compared to 2. Additionally, vitamin D receptor activity was
543 observed, which has been implicated in modulating the immune response and may
544 play a role in COVID-19 severity (41-43). Notably, this cluster exhibited low activation
545 of pathways related to TGF- β receptor signalling, IL1R signalling, and LTF danger
546 signal response. The reduced TGF- β receptor signalling suggests decreased fibrotic
547 response and tissue remodelling, while low IL1R signalling may indicate attenuated
548 inflammation (44). The activation of the LTF danger signal response pathway appears
549 to be diminished. Lactoferrin demonstrates antiviral capabilities against various
550 viruses, including coronaviruses (45). It can impede viral replication, disrupt viral
551 attachment and entry, and adjust host immune responses. Lactoferrin's
552 immunomodulatory attributes might aid in tempering excessive inflammation and
553 alleviating cytokine storms observed in severe cases of COVID-19 (46). The
554 decreased activation of the LTF danger signal response pathway could potentially
555 contribute to a weakened interferon response (47).

556

557 The stratified molecular phenotypes were found to have different expected responses
558 to both medicines used, and medicines not yet used for COVID-19 (Fig. 3). In cluster
559 1, CSA or cyclosporine has been shown to be safe to use during COVID-19 for the
560 intended use, however, a reduction in hyperinflammation was observed (48). This
561 warrants further investigation as highlighted by others (49). Interferon related therapies
562 that could modulate the pathway activation of cluster 1 were also identified, which have
563 been shown to have positive effects (50-52). Lifitegrast inhibits SARS-CoV-2 *in vitro*
564 (53, 54) By inhibiting TGF- β signalling, Luspatercept may help mitigate the excessive
565 inflammatory response and tissue damage seen in severe COVID-19 cases. Similarly,

566 Sargramostim has shown promise in a small study, but larger trials are needed to
567 confirm these findings (55).

568

569 Like, cluster 1, CSA was also identified as a potentially effective treatment for clusters
570 2 & 3. The mechanisms of actions of other medicines only matched the molecular
571 phenotype of cluster 2. Asenapine, an anti-psychotic drug identified by others as a
572 potential drug candidate for COVID-19 (56, 57) Cinryze a human c1 esterase inhibitor
573 was also identified, these inhibitors have been shown to improve lung computed
574 tomography scores and increase blood eosinophils, which are indicators of disease
575 recovery, however, time to clinical improvement was not observed (58). Also, for
576 cluster 2, we identified Fluoxetine and other SSRIs such as fluvoxamine which has
577 previously been identified as having potential use for the treatment of COVID-19 and
578 long-COVID (59) Amisulpride was also identified in cluster 3.

579

580 To further evaluate the utility of the TopMD algorithm for precision medicine,
581 enrichment analysis was performed on individual data from the 10 fatal cases within
582 the Florence and Liège cohorts. This approach highlights pathway activation specific
583 to each patient, bypassing the need for a whole cohort for deconvolution. All 10
584 patients showed potential therapeutic targets based on pathway enrichment. CXCR2
585 and GNAS were commonly activated across patients (Figure 5), suggesting drugs
586 such as Ibuprofen may be able to modulate some pathways associated with their
587 phenotype. For patients 2 and 6, ITGB2 emerged as one of the top druggable
588 pathways. Notably, Lifitegrast has shown to inhibit SARS-CoV-2 *in vitro* (53, 54).
589 Additionally, CSA or cyclosporine, was also identified, which was another compound
590 identified in the cluster analysis.

591

592 Multiple patients exhibited CSF2RB enrichment, indicating potential for Sargramostim,
593 a drug shown to reduce mortality and incubation in small COVID-19 study (55).
594 SERPING1 enrichment in 5 patients suggests various approved drugs for pathway
595 modulation, including antithrombin, human c1 esterase inhibitor and cinryze. Patient
596 specific findings were also observed. PIK3CD enrichment in patient 5 suggests
597 Sophoretin as a potentially modulator, with a meta-analysis showing quercetins
598 (including sophoretin), reduce LDH, hospitalisation risk and mortality (60). Patient 9
599 displayed TGFBR2 enrichment indicating luspatercept as a potential drug (identified

600 in the cluster analysis) as a potential candidate. Lastly, CUL4B enrichment in patient
601 10, suggests Thalidomide, Pomalidomide, Lenalidomide for pathway modulation.
602 While Lenalidomide, used to manage multiple myelomas, has been proposed as
603 protective against severe COVID-19 in a case report (61) a clinical trial showed no
604 benefit (62). Thalidomide, although showing no benefit itself (62), remains a subject of
605 discussion for its potential use in COVID-19 (63).

606

607 As a proof of concept, TopMD models were integrated into the Comunicare platform
608 (27), a tool developed and configured within the framework of the DRAGON project,
609 aimed at patient empowerment and providing disease management tooling for
610 clinicians and patients. This proof of concept also enables the analysis of clinical data
611 for clinicians in a dedicated dashboard to demonstrate the possibilities of
612 transcriptomics in digital health. As an example, we generated a model that predicts
613 ICU admission based on our previous work (5) as other outcome variables were too
614 low in number. If a clinician has access to transcriptomic data, a csv file can be
615 uploaded to the dashboard and in return activated pathways are returned after running
616 analysis on the TopMD API. While the use of transcriptomics at the bedside is not
617 ready for deployment, we propose that it is a major advance to be able to demonstrate
618 integration of this data into digital health platforms as the growth of precision medicine
619 continues.

620

621 This study identified three distinct molecular phenotypes in hospitalised COVID-19
622 patients, which were not associated with differences in CT scans and clinical
623 observations. However, these molecular phenotypes match the mechanism of action
624 of different medicines, providing the opportunity for biomarker-led stratified medicine.
625 Topological analysis of global gene expression to define a patient's pathway activation
626 map could be useful in future pandemics to aid in treatment decisions before clinical
627 trials can be completed.

628

629 **Funding:**

630 TopMD, the University of Southampton, Imperial College London, CDISC,
631 Comunicare Solutions, and the University of Liverpool are members of the DRAGON
632 consortium. The DRAGON project has received funding from the Innovative Medicines
633 Initiative 2 Joint Undertaking (JU) under grant agreement No 101005122. The JU
634 receives support from the European Union's Horizon 2020 research and innovation
635 program and EFPIA. This publication reflects the author's view. Neither IMI nor the
636 European Union, EFPIA or the DRAGON consortium, are responsible for any use that
637 may be made of the information contained therein. JAH, TP, RPR and CH were
638 supported by the US Food and Drug Administration Medical Countermeasures
639 Initiative (no 75F40120C00085) awarded to JAH and work was also supported by the
640 MRC funded MR/Y004205/1 'The G2P2 virology consortium'. The funders had no role
641 in study design, data collection and analysis, decision to publish, or preparation of the
642 manuscript. DB is funded by NIHR and MRC.

643

644 **Acknowledgments:**

645 The authors wish to thank the study participants and the hospital staff for their
646 participation in this study.

647

648 **Contributions:**

649 RPR, FS: methodology, RPR, FS: visualisation, RPR, FS, BVE, TK: software, BE:
650 project administration, RPR, FS, JG, MH, AS, EG, AFD, LG, AJP, CN: investigation,
651 RPR, FS, JG, CH, TP, SW: formal analysis, JG, CN: clinical supervision, RPR, FS,
652 AJP, ST, RB, KH, XX, YN, SW: data curation, RPR, FS, EP, PS, JAH, JPS: writing -
653 original draft preparation, RPR, FB, BE, BE, JG, MH, AS, EG, AFD, LG, AJP, CN, ST,
654 RB, KH, CH, TP, RD, TC, DB, SW, XX, YN, SW, SW, GY, PJS, JAH, JPRS: writing -
655 review and editing, JPRS, JAH, PJS, GY, SW: funding acquisition

656

657 **Declarations:**

658 RPR is an employee at TopMD Precision Medicine Ltd. JPRS is a founding director,
659 CEO, employee, and shareholder in TopMD Precision Medicine Ltd. FS is a founding
660 director, CTO, employee, and shareholder in TopMD Precision Medicine Ltd. PS is a

661 founding director, employee, and shareholder in TopMD Precision Medicine Ltd. BVE
662 is CEO of Comunicare Solutions. TK is CTO of Comunicare Solutions.

663 **Data availability:**

664

665 Sequencing reads available under SRA bioproject: PRJNA1085259

666 **References:**

- 667 1. Clark JJ, Penrice-Randal R, Sharma P, Kipar A, Dong X, Pennington SH, et
668 al. Sequential infection with influenza A virus followed by severe acute respiratory
669 syndrome coronavirus 2 (SARS-CoV-2) leads to more severe disease and
670 encephalitis in a mouse model of COVID-19. *bioRxiv*. 2023:2020.10.13.334532.
- 671 2. De Neck S, Penrice-Randal R, Clark JJ, Sharma P, Bentley EG, Kirby A, et al.
672 The Stereotypic Response of the Pulmonary Vasculature to Respiratory Viral
673 Infections: Findings in Mouse Models of SARS-CoV-2, Influenza A and
674 Gammaherpesvirus Infections. *Viruses* [Internet]. 2023; 15(8).
- 675 3. Dorward DA, Russell CD, Um IH, Elshani M, Armstrong SD, Penrice-Randal
676 R, et al. Tissue-Specific Immunopathology in Fatal COVID-19. *Am J Respir Crit Care*
677 *Med*. 2021;203(2):192-201.
- 678 4. Legebeke J, Lord J, Penrice-Randal R, Vallejo AF, Poole S, Brendish NJ, et
679 al. Evaluating the Immune Response in Treatment-Naive Hospitalised Patients With
680 Influenza and COVID-19. *Front Immunol*. 2022;13:853265.
- 681 5. Penrice-Randal R, Dong X, Shapanis AG, Gardner A, Harding N, Legebeke J,
682 et al. Blood gene expression predicts intensive care unit admission in hospitalised
683 patients with COVID-19. *Front Immunol*. 2022;13:988685.
- 684 6. Russell CD, Valanciute A, Gachanja NN, Stephen J, Penrice-Randal R,
685 Armstrong SD, et al. Tissue Proteomic Analysis Identifies Mechanisms and Stages
686 of Immunopathology in Fatal COVID-19. *Am J Respir Cell Mol Biol*. 2021.
- 687 7. Liu X, Speranza E, Muñoz-Fontela C, Haldenby S, Rickett NY, Garcia-Dorival
688 I, et al. Transcriptomic signatures differentiate survival from fatal outcomes in
689 humans infected with Ebola virus. *Genome Biology*. 2017;18(1):4.
- 690 8. McClain MT, Constantine FJ, Nicholson BP, Nichols M, Burke TW, Henao R,
691 et al. A blood-based host gene expression assay for early detection of respiratory
692 viral infection: an index-cluster prospective cohort study. *Lancet Infect Dis*.
693 2021;21(3):396-404.
- 694 9. Carroll MW, Matthews DA, Hiscox JA, Elmore MJ, Pollakis G, Rambaut A, et
695 al. Temporal and spatial analysis of the 2014-2015 Ebola virus outbreak in West
696 Africa. *Nature*. 2015;524(7563):97-101.
- 697 10. Watson RJ, Tree J, Fotheringham SA, Hall Y, Dong X, Steeds K, et al. Dose-
698 Dependent Response to Infection with Ebola Virus in the Ferret Model and Evidence
699 of Viral Evolution in the Eye. *Journal of virology*. 2021;95(24):e0083321.
- 700 11. Russell CD, Valanciute A, Gachanja NN, Stephen J, Penrice-Randal R,
701 Armstrong SD, et al. Tissue proteomic analysis identifies mechanisms and stages of
702 immunopathology in fatal COVID-19. *American journal of respiratory cell and*
703 *molecular biology*. 2022;66(2):196-205.
- 704 12. Nan Y, Ser JD, Walsh S, Schönlieb C, Roberts M, Selby I, et al. Data
705 harmonisation for information fusion in digital healthcare: A state-of-the-art
706 systematic review, meta-analysis and future research directions. *Information Fusion*.
707 2022;82:99-122.
- 708 13. Halilaj I, Chatterjee A, van Wijk Y, Wu G, van Eeckhout B, Oberije C, et al.
709 Covid19Risk.ai: An Open Source Repository and Online Calculator of Prediction
710 Models for Early Diagnosis and Prognosis of Covid-19. *BioMed*. 2021;1(1):41-9.
- 711 14. Chatterjee A, Wu G, Primakov S, Oberije C, Woodruff H, Kubben P, et al. Can
712 predicting COVID-19 mortality in a European cohort using only demographic and
713 comorbidity data surpass age-based prediction: An externally validated study. *PLOS*
714 *ONE*. 2021;16(4):e0249920.

- 715 15. Cen X, Wang F, Huang X, Jovic D, Dubee F, Yang H, et al. Towards precision
716 medicine: Omics approach for COVID-19. *Biosaf Health*. 2023;5(2):78-88.
- 717 16. Teodori L, Osimani B, Isidoro C, Ramakrishna S. Mass versus personalized
718 medicine against COVID-19 in the “system sciences” era. *Cytometry Part A*.
719 2022;101(12):995-9.
- 720 17. Wang Z, He Y. Precision omics data integration and analysis with
721 interoperable ontologies and their application for COVID-19 research. *Briefings in*
722 *Functional Genomics*. 2021;20(4):235-48.
- 723 18. Venkataraman T, Coleman CM, Frieman MB. Overactive Epidermal Growth
724 Factor Receptor Signaling Leads to Increased Fibrosis after Severe Acute
725 Respiratory Syndrome Coronavirus Infection. *Journal of virology*. 2017;91(12).
- 726 19. Venkataraman T, Frieman MB. The role of epidermal growth factor receptor
727 (EGFR) signaling in SARS coronavirus-induced pulmonary fibrosis. *Antiviral Res*.
728 2017;143:142-50.
- 729 20. Vagapova ER, Lebedev TD, Prassolov VS. Viral fibrotic scoring and drug
730 screen based on MAPK activity uncovers EGFR as a key regulator of COVID-19
731 fibrosis. *Scientific Reports*. 2021;11(1):11234.
- 732 21. Chen S, Zhou Y, Chen Y, Gu J. fastp: an ultra-fast all-in-one FASTQ
733 preprocessor. *Bioinformatics*. 2018;34(17):i884-i90.
- 734 22. Patro R, Duggal G, Love MI, Irizarry RA, Kingsford C. Salmon provides fast
735 and bias-aware quantification of transcript expression. *Nature Methods*.
736 2017;14(4):417-9.
- 737 23. Soneson C, Love MI, Robinson MD. Differential analyses for RNA-seq:
738 transcript-level estimates improve gene-level inferences. *F1000Res*. 2015;4:1521.
- 739 24. Robinson MD, McCarthy DJ, Smyth GK. edgeR: a Bioconductor package for
740 differential expression analysis of digital gene expression data. *Bioinformatics*.
741 2010;26(1):139-40.
- 742 25. Szklarczyk D, Kirsch R, Koutrouli M, Nastou K, Mehryary F, Hachilif R, et al.
743 The STRING database in 2023: protein-protein association networks and functional
744 enrichment analyses for any sequenced genome of interest. *Nucleic Acids Res*.
745 2023;51(D1):D638-d46.
- 746 26. Freshour SL, Kiwala S, Cotto KC, Coffman AC, McMichael JF, Song JJ, et al.
747 Integration of the Drug-Gene Interaction Database (DGIdb 4.0) with open
748 crowdsource efforts. *Nucleic Acids Res*. 2021;49(D1):D1144-d51.
- 749 27. Duquenne JB, Corhay JL, Louis R, Van Cauwenberge H. [Feasibility and
750 effectiveness study of a simplified mobile self-education and self-monitoring
751 application for patients with severe chronic obstructive pulmonary disease]. *Rev Med*
752 *Liege*. 2022;77(2):110-7.
- 753 28. Farahani M, Niknam Z, Mohammadi Amirabad L, Amiri-Dashatan N, Koushki
754 M, Nemati M, et al. Molecular pathways involved in COVID-19 and potential
755 pathway-based therapeutic targets. *Biomedicine & Pharmacotherapy*.
756 2022;145:112420.
- 757 29. Guiot J, Vaidyanathan A, Deprez L, Zerka F, Danthine D, Frix A-N, et al.
758 Development and Validation of an Automated Radiomic CT Signature for Detecting
759 COVID-19. *Diagnostics*. 2021;11(1):41.
- 760 30. Guiot J, Maes N, Winandy M, Henket M, Ernst B, Thys M, et al. Automated
761 lung disease quantification in patients with COVID-19 as a predictive tool to assess
762 hospitalization severity. *Frontiers in Medicine*. 2022;9.

- 763 31. Carpenè G, Onorato D, Nocini R, Fortunato G, Rizk JG, Henry BM, et al.
764 Blood lactate concentration in COVID-19: a systematic literature review. *Clin Chem*
765 *Lab Med*. 2022;60(3):332-7.
- 766 32. Chen W, Liu H, Yang G, Wang W, Liu Q, Huang C, et al. Effect of Direct
767 Bilirubin Level on Clinical Outcome and Prognoses in Severely/Critically Ill Patients
768 With COVID-19. *Front Med (Lausanne)*. 2022;9:843505.
- 769 33. Garvin MR, Alvarez C, Miller JI, Prates ET, Walker AM, Amos BK, et al. A
770 mechanistic model and therapeutic interventions for COVID-19 involving a RAS-
771 mediated bradykinin storm. *Elife*. 2020;9.
- 772 34. Lee C. Therapeutic Modulation of Virus-Induced Oxidative Stress via the Nrf2-
773 Dependent Antioxidative Pathway. *Oxid Med Cell Longev*. 2018;2018:6208067.
- 774 35. Chen J, Wu W, Wang W, Tang Y, Lan H-Y. Role of TGF- β Signaling in
775 Coronavirus Disease 2019. *Integrative Medicine in Nephrology and Andrology*.
776 2022;9(1):9.
- 777 36. Conway EM, Mackman N, Warren RQ, Wolberg AS, Mosnier LO, Campbell
778 RA, et al. Understanding COVID-19-associated coagulopathy. *Nat Rev Immunol*.
779 2022;22(10):639-49.
- 780 37. Fattahi S, Khalifehzadeh-Esfahani Z, Mohammad-Rezaei M, Mafi S, Jafarinia
781 M. PI3K/Akt/mTOR pathway: a potential target for anti-SARS-CoV-2 therapy.
782 *Immunol Res*. 2022;70(3):269-75.
- 783 38. Khezri MR, Varzandeh R, Ghasemnejad-Berenji M. The probable role and
784 therapeutic potential of the PI3K/AKT signaling pathway in SARS-CoV-2 induced
785 coagulopathy. *Cell Mol Biol Lett*. 2022;27(1):6.
- 786 39. Kindrachuk J, Ork B, Hart BJ, Mazur S, Holbrook MR, Frieman MB, et al.
787 Antiviral potential of ERK/MAPK and PI3K/AKT/mTOR signaling modulation for
788 Middle East respiratory syndrome coronavirus infection as identified by temporal
789 kinome analysis. *Antimicrob Agents Chemother*. 2015;59(2):1088-99.
- 790 40. Channappanavar R, Perlman S. Pathogenic human coronavirus infections:
791 causes and consequences of cytokine storm and immunopathology. *Semin*
792 *Immunopathol*. 2017;39(5):529-39.
- 793 41. Azmi A, Rismani M, Pourmontaseri H, Mirzaii E, Niknia S, Miladpour B. The
794 role of vitamin D receptor and IL-6 in COVID-19. *Mol Genet Genomic Med*.
795 2023;11(7):e2172.
- 796 42. Hurst EA, Mellanby RJ, Handel I, Griffith DM, Rossi AG, Walsh TS, et al.
797 Vitamin D insufficiency in COVID-19 and influenza A, and critical illness survivors: a
798 cross-sectional study. *BMJ Open*. 2021;11(10):e055435.
- 799 43. Evans RM, Lippman SM. Shining Light on the COVID-19 Pandemic: A
800 Vitamin D Receptor Checkpoint in Defense of Unregulated Wound Healing. *Cell*
801 *Metabolism*. 2020;32(5):704-9.
- 802 44. Biernacka A, Dobaczewski M, Frangogiannis NG. TGF- β signaling in fibrosis.
803 *Growth Factors*. 2011;29(5):196-202.
- 804 45. Puddu P, Valenti P, Gessani S. Immunomodulatory effects of lactoferrin on
805 antigen presenting cells. *Biochimie*. 2009;91(1):11-8.
- 806 46. Zimecki M, Actor JK, Kruzel ML. The potential for Lactoferrin to reduce SARS-
807 CoV-2 induced cytokine storm. *Int Immunopharmacol*. 2021;95:107571.
- 808 47. Actor JK, Hwang SA, Kruzel ML. Lactoferrin as a natural immune modulator.
809 *Curr Pharm Des*. 2009;15(17):1956-73.
- 810 48. Blumberg EA, Noll JH, Tebas P, Fraietta JA, Frank I, Marshall A, et al. A
811 phase I trial of cyclosporine for hospitalized patients with COVID-19. *JCI Insight*.
812 2022;7(11).

- 813 49. Devaux CA, Melenotte C, Piercecchi-Marti MD, Delteil C, Raoult D.
814 Cyclosporin A: A Repurposable Drug in the Treatment of COVID-19? *Front Med*
815 (Lausanne). 2021;8:663708.
- 816 50. Kamyshnyi A, Koval H, Kobevko O, Buchynskiy M, Oksenysh V, Kainov D, et
817 al. Therapeutic Effectiveness of Interferon- α 2b against COVID-19 with Community-
818 Acquired Pneumonia: The Ukrainian Experience. *Int J Mol Sci*. 2023;24(8).
- 819 51. Reis G, Moreira Silva EAS, Medeiros Silva DC, Thabane L, Campos VHS,
820 Ferreira TS, et al. Early Treatment with Pegylated Interferon Lambda for Covid-19.
821 *New England Journal of Medicine*. 2023;388(6):518-28.
- 822 52. Monk PD, Marsden RJ, Tear VJ, Brookes J, Batten TN, Mankowski M, et al.
823 Safety and efficacy of inhaled nebulised interferon beta-1a (SNG001) for treatment
824 of SARS-CoV-2 infection: a randomised, double-blind, placebo-controlled, phase 2
825 trial. *The Lancet Respiratory Medicine*. 2021;9(2):196-206.
- 826 53. Shen X-R, Geng R, Li Q, Chen Y, Li S-F, Wang Q, et al. ACE2-independent
827 infection of T lymphocytes by SARS-CoV-2. *Signal Transduction and Targeted*
828 *Therapy*. 2022;7(1):83.
- 829 54. Day CJ, Bailly B, Guillon P, Dirr L, Jen FE, Spillings BL, et al. Multidisciplinary
830 Approaches Identify Compounds that Bind to Human ACE2 or SARS-CoV-2 Spike
831 Protein as Candidates to Block SARS-CoV-2-ACE2 Receptor Interactions. *mBio*.
832 2021;12(2).
- 833 55. Paine R, Chasse R, Halstead ES, Nfonoyim J, Park DJ, Byun T, et al. Inhaled
834 Sargramostim (Recombinant Human Granulocyte-Macrophage Colony-Stimulating
835 Factor) for COVID-19-Associated Acute Hypoxemia: Results of the Phase 2,
836 Randomized, Open-Label Trial (iLeukPulm). *Mil Med*. 2022;188(7-8):e2629-38.
- 837 56. Ku KB, Shin HJ, Kim HS, Kim BT, Kim SJ, Kim C. Repurposing Screens of
838 FDA-Approved Drugs Identify 29 Inhibitors of SARS-CoV-2. *J Microbiol Biotechnol*.
839 2020;30(12):1843-53.
- 840 57. Rajput A, Thakur A, Rastogi A, Choudhury S, Kumar M. Computational
841 identification of repurposed drugs against viruses causing epidemics and pandemics
842 via drug-target network analysis. *Comput Biol Med*. 2021;136:104677.
- 843 58. Mansour E, Palma AC, Ulaf RG, Ribeiro LC, Bernardes AF, Nunes TA, et al.
844 Safety and Outcomes Associated with the Pharmacological Inhibition of the Kinin-
845 Kallikrein System in Severe COVID-19. *Viruses*. 2021;13(2).
- 846 59. Hashimoto K. Overview of the potential use of fluvoxamine for COVID-19 and
847 long COVID. *Discov Ment Health*. 2023;3(1):9.
- 848 60. Ziaei S, Alimohammadi-Kamalabadi M, Hasani M, Malekahmadi M, Persad E,
849 Heshmati J. The effect of quercetin supplementation on clinical outcomes in COVID-
850 19 patients: A systematic review and meta-analysis. *Food Science & Nutrition*.
851 2023;11(12):7504-14.
- 852 61. Al Sbihi A, Manasrah N, Sano D. Can Lenalidomide Protect against Severe
853 COVID-19 Symptoms in Multiple Myeloma Patients? A Case Series and Review of
854 the Literature. *Eur J Case Rep Intern Med*. 2022;9(3):003216.
- 855 62. Amra B, Ashrafi F, Torki M, Hashemi M, Shirzadi M, Soltaninejad F, et al.
856 Thalidomide for the Treatment of COVID-19 Pneumonia: A Randomized Controlled
857 Clinical Trial. *Adv Biomed Res*. 2023;12:14.
- 858 63. Sundaresan L, Giri S, Singh H, Chatterjee S. Repurposing of thalidomide and
859 its derivatives for the treatment of SARS-coV-2 infections: Hints on molecular action.
860 *Br J Clin Pharmacol*. 2021;87(10):3835-50.
- 861